

Scale Effects on Ducted Propellers

M. Abdel-Maksoud, H.-J. Heinke
(Potsdam Model Basin, SVA)

ABSTRACT

For certain applications, ducted propellers have advantages in comparison to free running propellers, especially in case of high loading coefficients or strong in-homogeneity of the inflow. In both cases, there is a strong effect of the viscosity on the propeller performance. An accurate estimation of the Reynolds number effect on the performance of propellers is very important for extrapolation of the model results to full-scale.

Results of numerical calculations for a ducted propeller are presented for model and full-scale. The numerical full-scale results show that the flow velocity in the nozzle is comparatively higher than in model scale. This fact leads to an increase of the nozzle thrust and to a reduction of the thrust and of the torque of the propeller. The influence of the Reynolds number on the torque of a ducted propeller is consequently higher than on a free running propeller. That may be an explanation for often observed too light loaded propellers in full-scale which were designed on the basis of test results in model scale.

INTRODUCTION

In fact, long experience and well established methods are available for considering the scale effect on the characteristic of free running propellers, e.g. the ITTC 1978 method. Increasing the Reynolds number leads to an increase of the thrust coefficient and to a decrease of the torque coefficient. The effect of the Reynolds number on the torque coefficient is much higher than on the thrust coefficient. The reason is that friction forces have more influence on the torque than on the thrust. The estimation of the scale effects for ducted propellers is not a straightforward subject. The nozzle is a part of the propulsion system, which may produce more thrust than the propeller at bollard pull condition. The strong interaction between the nozzle and the propeller is dependent on the Reynolds number. The inflow of the propeller is directly effected by the form of the nozzle and vice versa.

The report of the specialist committee for unconventional propulsors of the 22nd ITTC focused the problem of the extrapolation of powering performance of ducted propellers, ITTC (1999). The three methods presented by Stierman (1984) were discussed. In the first one the nozzle is considered as an appendage of the hull, in the second one as a part of the propulsion system. The last method considers

the interaction between three objects: ship, nozzle and propeller.

The investigation of a hull fitted with a nozzle alone (without propeller) as the case in the first and the third method, will lead to limited informative results. The flow around the propeller or the nozzle alone differs totally from the flow around the ducted propeller system. Therefore the drawback in the first and the third method is the weak consideration of the interaction between the nozzle and the propeller.

In the second method of Stierman (1984) the thrust of the nozzle and of the propeller are scaled separately. The extrapolation of the propeller characteristics is carried out using the ITTC 1978 method. The resistance of the nozzle is corrected by employing a flat plate friction line or a formula according to Hoerner. The resistance of the nozzle can be measured at zero thrust of the propeller. The drawback of this method is that the flow around the nozzle is strongly dependent on the thrust loading coefficient of the propeller. The consideration of the information on the flow around the nozzle at a very low propeller loading coefficient in order to correct the nozzle thrust at a high loading condition will lead to more inaccuracies in the results. At high loading conditions the ratio of the friction resistance of the nozzle to the nozzle thrust is very small. This means that this correction will have nearly no influence on the nozzle thrust.

It is known in the practice that in some cases full-scale ducted propellers are not able to absorb the available torque at the given number of revolutions. This means that full-scale propellers are loaded lightly than expected according to model test results. The variation of the thrust-torque ratio between model and full-scale shows a certain influence of the Reynolds number on the performance of the ducted propeller, which cannot be covered or explained by the available extrapolation methods. The weak consideration of the scale effect on the nozzle performance and the interaction parameter between nozzle and propeller may be responsible for the discrepancies between model and full-scale results.

The aim of the presented study is the investigation of the flow at different Reynolds numbers and loading conditions. This is helpful to have a better understanding of the flow behaviour on ducted propellers and to improve the accuracy of the extrapolation methods.

The experimental and numerical investigations for improving the performance of ducted propellers have been intensified during the recent years. The main aim of this research work was the optimisation of the nozzle and the propeller. Achieving a high

total thrust coefficient under the bollard pull condition is often an important criterion for the operation of ducted propellers. In model scale, the results of the open water tests are adequate to compare different designs. The extrapolation of the measured results from model to full-scale is not a straightforward task, because the results are directly effected by the employed assumptions of the Reynolds number effects.

Viscous flow methods can be applied to overcome this drawback and to have more detailed information on the viscous flow through and around ducted propellers in model and full-scale. The comparison of the numerical results for model and full-scale is very helpful for the analysis of scale effects.

The examination of scale effects requires a high quality of the numerical results. Therefore many investigations have been carried out to study the effect of different boundary conditions, the size of the calculation domain and the topology of the numerical grid on the numerical results.

NUMERICAL CALCULATION

The calculation of the viscous flow on a ducted propeller is more complicated than that on a free running propeller. Convergence problems may take place at high thrust loading coefficients. The convergence problems are raised due to the extreme ratio between the inflow velocity and the circumferential speed as well as the high difference between the velocity at the inlet of the calculation domain and the inflow velocity of the propeller. While the first one is independent on the simulation time t_s , the inflow velocity to the propeller is simulation time dependent. The ratio between the nozzle and propeller thrust and thus the amount of the total thrust of the ducted propeller system and the torque of the propeller changes significantly at the beginning of the simulation, see Figure 1. The high circumferential speed of the propeller and the flow in the gap between the blade tip and nozzle are also problematic for the convergence behaviour of the calculation.

In case of a ducted propeller working in a homogeneous flow, the calculation domain is periodic in space and the calculation may be restricted to one propeller blade. The interaction with other blades can be considered by a periodic boundary condition. In this case, the calculation domain is divided into a stationary part and a rotating part. The last one contains the propeller region of the numerical grid. A cartesian co-ordinate system is applied to the stationary part. The flow around the propeller is calculated in a rotating co-ordinate system. A sliding interface is defined between the rotating and the fixed numerical grid.

The RANS equations in a rotating co-ordinate system involve additional terms for the centrifugal and coriolis forces (Abdel-Maksoud, Menter and Wuttke 1998). The velocity vector in the inertial

system C_i can be divided into a velocity vector in the rotating system W_i and the velocity vector due to the rotation of the system U_i as follows:

$$C_i = W_i + U_i \quad (1)$$

Capital letters refer to time averaged variables. The speed of rotation is defined as:

$$U_i = e_{ijk} \omega_j \chi_k \quad (2)$$

In this equation the permutation tensor e_{ijk} is used

$$e_{ijk} = \begin{cases} +1 & \text{for } ijk \text{ cyclic,} \\ -1 & \text{for } ijk \text{ anticyclic,} \\ 0 & \text{for } ijk \text{ all other combinations.} \end{cases} \quad (3)$$

The equation for the conservation of mass reads:

$$\frac{\partial \rho}{\partial t} + \frac{\partial (\rho C_j)}{\partial \chi_j} = 0 \quad (4)$$

The momentum equations in a rotating system are:

$$\frac{\partial (\rho W_j)}{\partial t} + \frac{\partial (\rho W_j C_i)}{\partial \chi_j} = - \frac{\partial P}{\partial \chi_i} - \frac{\partial (\overline{\tau_{ij} + \rho w_i w_j})}{\partial \chi_j} - \rho e_{ijk} \omega_j C_k \quad (5)$$

This form of the equations is optimal for the numerical simulation of flows with strong relative rotation between the co-ordinate system and the fluid. The overbar refers to time averages of the turbulent variables. The viscous stress tensor is:

$$\tau_{ij} = -\mu \left(\frac{\partial W_i}{\partial \chi_j} + \frac{\partial W_j}{\partial \chi_i} \right) \quad (6)$$

The standard $k-\varepsilon$ model in combination with wall function or the SST model can be applied to consider the effects of turbulence on the flow. The SST model combines the $k-\varepsilon$ and $k-\omega$ models. For the free stream region the $k-\varepsilon$ model is used and for the near wall flow region the $k-\omega$ model is applied, (Menter 1994). The strong variation of the local velocity distribution on the duct and on the propeller leads to strong fluctuations of velocity near the wall region. The treatment of the boundary conditions near the wall must be able to handle this problem without losses of robustness or accuracy of the numerical solution. The local tangential velocity component u_T at the first node of the numerical grid and the distance of the first node from the wall Δn are used to define the dimensionless distance from the wall y^+ as follows:

$$y^+ = \frac{\rho \Delta n u_T}{\mu} \quad (7)$$

For the application of the logarithmic wall function the y^+ value should be higher than 11. Due to the strong variation of the velocity near the wall the applied numerical method must be able to handle small y^+ values. This problem can be solved by applying the scalable wall function technology, (Grotjans and Menter, 1998). Another way to overcome the problem is to switch between the $k-\omega$ model at small y^+ values and the wall function at high values of it.

The CFX-TASCflow solution method is applied at the Potsdam Model Basin SVA, (Abdel-Maksoud and Heinke, 2000). The numerical solution is based on the conservative finite volume method, (Raw, 1995). The code has been optimised and intensively tested for different applications such as a propeller in uniform flow and a ship with rotating propeller flow, (Abdel-Maksoud, Rieck and Menter, 2000). This work was part of long-term co-operative research activities between the Potsdam Model Basin and AEA Technology Otterfing GmbH. The German Ministry for Education and Research kindly sponsored the research projects.

The numerical method includes fully conservative stage capabilities to simulate the interaction of the propeller and the propulsion system, (Menter, Abdel-Maksoud and Galpin, 1998). The discretisation in space is based on a block-structured finite volume grid around the duct and the blade of the propeller. The faces of the control volumes at the interface between the rotating and the stationary frame can be non-matching. The applied code is able to handle non-overlapping non-matching grid interfaces.

EXAMINATION OF THE BOUNDARY CONDITIONS

The impact of boundary and initial conditions and the local optimisation of the numerical grid on the results of the calculation have been studied on a ducted propeller system, (Abdel-Maksoud 2000). A 3D CAD model was applied to generate the numerical grid. The CAD model contained the nozzle and propeller geometry without simplification. The gap between the blade tip and the cylindrical part of the nozzle was considered. The numerical calculation was executed with two numerical grids. Each consisted of 25 blocks. The first one contained 320,000 nodes for one propeller blade and the second one twice as much. Not only the resolution of the numerical grid was varied but also its topology. A simulation period of approx. 30 seconds was applied to all calculations.

The boundary conditions of the calculation have been studied for various thrust loading coefficients. The results of five calculations with different

turbulence models and/or dimensions of the calculation domain for the thrust loading coefficient $C_{Th} = 1000$ of the ducted propeller system are shown in Table 1. The evaluation of the numerical results of the different cases is given in Abdel-Maksoud (2000). The results of the study show that for $C_{Th} = 1000$ a certain dimension of the calculation domain should be maintained to avoid any influence on the numerical results. The dimensions are given as a ratio of the propeller diameter D . The position of the inflow plane should be located at $87 D$, the outflow plane at $130.5 D$. The diameter of the calculation domain should be at least $70 D$.

The comparison between the $k-\varepsilon$ and SST turbulence model shows that better results can be achieved by employing the SST model in particular for a separated flow, which is the case at a high thrust loading coefficient. The numerical grid of the fifth case was optimised to achieve the requirements of the SST model. The numerical results of the fifth case show a good agreement with the measured coefficients of the ducted propeller system, see Table 1.

NUMERICAL INVESTIGATIONS

The numerical investigations were carried out for one propeller geometry and one nozzle form. The geometry of the Wageningen 19A nozzle and Wageningen KA 5-75 propeller were selected for the investigations. The computations were carried out for four propeller diameters ($D = D_M = 0.201$ m and $D = D_S = 1.005, 2.01, 4.02$ m) and four different thrust loading coefficients ($C_{Th} \approx 4.25, 8.5, 85$ and 850). The data of the propeller and nozzle are given in the Tables 2 and 3 for the diameter $D_M = 0.201$ m.

In all numerical calculations the SST turbulence model was applied. The numerical grid in the near wall region was modified for each Reynolds number in order to improve the distribution of grid points in the boundary layer. The number of grid nodes and topology of the grid were kept constant during the computation. The number of nodes of the applied grid for one propeller blade was 821,718. The multiblock grid consisted of 26 blocks. Figure 2 shows the numerical grid on the nozzle and the geometry of the investigated configuration.

OPEN WATER CHARACTERISTICS

Figure 3 shows a comparison of the coefficients of the propeller KA 5-75 working in the nozzle Wag. 19A, calculated with CFX-TASCflow and with the polynomial coefficients of Wageningen PSP version 1.02, (Kuiper, 1992).

The agreement between the coefficients of the numerical calculations and the polynomial coefficients from MARIN is good. The numerical results confirm that CFD calculations with ducted propellers are possible for high thrust loading coefficients ($C_{Th} \leq 1000$) and also for reversed

direction of rotation of the propeller (the ducted propeller is working backwards).

The knowledge acquired in the systematic investigations of the boundary conditions, the optimisation of the numerical grid, the analyses of calculated and measured characteristics of ducted propellers and the study of local velocity fields was very important to achieve accurate results for the calculation of ducted propellers.

FLOW DETAILS

The velocity vectors for each thrust loading coefficient and scale ratio are shown in Figures 4 to 19. The velocity vectors are presented on different selected regions on the ducted propeller such as: on the outside wall of the nozzle profile, near the leading and trailing edges of the nozzle and in the region of the gap between the propeller blade and nozzle.

The results for $C_{Th} = 4.25$ are shown in Figures 4 to 7. The velocity distribution on the outside wall of the nozzle is presented in Figure 4. In model scale ($D_M = 0.201$ m) the velocity vectors have the expected character of low Reynolds number velocity profiles with a thick boundary layer in comparison to scale ratios $\lambda = 4, 2$ and 1. Figure 5 shows the velocity vectors near the leading edge of the nozzle, as it is expected, a separation may take place near the leading edge of the nozzle of the model at a low thrust coefficient. This separation region disappears with increasing the Reynolds number of the investigated ducted propeller see Figure 5.

Figure 6 shows the velocity vectors near the trailing edge of the nozzle. It can be seen that the thickness of the boundary layer and the size of the separation region behind the nozzle decrease at high Reynolds numbers. The velocity vectors in the tip region of the blade are shown in Figure 7. The tip vortex is directly effected by the thickness of the boundary layer on the inside wall of the nozzle. The relatively low velocity in the boundary layer in model scale increases the thrust loading of the propeller blade near the tip. Therefore, it should be expected that the influence of the Reynolds number on the behaviour of the tip vortex of a ducted propeller and of a free running one is completely different.

The results for $C_{Th} = 8.5$ are presented in Figures 8 to 11. The comparison between velocity vectors on the outside wall of the nozzle at different Reynolds numbers shows the relatively higher thickness of the boundary layer in model scale, Figure 8. It can be seen that the acceleration of the flow on the leading edge of the nozzle increases with increasing the Reynolds number. Due to the increase in the thrust loading the axial velocity component outside the nozzle at $C_{Th} = 8.5$ (Figures 8 and 9) is smaller than at $C_{Th} = 4.25$ (Figures 4 and 5).

Figure 10 shows the velocity vectors near the trailing edge of the nozzle at $C_{Th} = 8.5$. The

separation point moves to the trailing edge and the size of the separation region behind the nozzle decreases with increasing the Reynolds number. The influence of the Reynolds number on the behaviour of the tip vortex can be seen in Figure 11. The difference in the tip vortex between model and full-scale will be smaller with increasing the thrust loading. The reason is that with increasing the thrust loading the thickness of the boundary layer on the inside wall of the nozzle decreases due to the higher acceleration of the flow through the nozzle. This effect reduces the thrust loading of the tip of the propeller blades.

The results for $C_{Th} = 85$ and 850 are shown in Figures 12 to 19. With increasing the thrust loading coefficient the location of the stagnation point moves on the outside wall of the nozzle in the direction of the trailing edge. The acceleration of the flow on the nozzle also increases at high Reynolds numbers, which means that more pressure reduction on the nozzle and more nozzle thrust should be expected. Figures 14 and 18 show that the separation region behind the nozzle is reduced by increasing the thrust loading, compare the corresponding results at $C_{Th} = 4.25$ and 8.5.

REYNOLDS NUMBER EFFECTS

The differences of the flow behaviour around the ducted propeller at the different scales have a strong influence on the performance characteristic of the propeller and nozzle.

Figure 20 shows the calculated changes of the propeller and nozzle coefficients due to the Reynolds number effect. The coefficients K_{TPS} , K_{QS} and K_{TNS} for the propeller diameters $D_S = 1.005, 2.01$ and 4.02 m are given in relation to the coefficients K_{TPM} , K_{QM} and K_{TNM} for the propeller diameters $D_M = 0.201$ m.

The thrust of the nozzle is increasing with the rising of the Reynolds number ($K_{TNS}/K_{TNM} = 1.03 - 1.10$) for the investigated thrust loading coefficients. The change in the nozzle thrust coefficients depends on the difference in Reynolds number and the flow around the nozzle, characterised by the thrust loading coefficient. The Reynolds number effect on the nozzle thrust is stronger for low thrust loading coefficients.

The thrust coefficients of the propeller are decreasing due to the Reynolds number effect ($K_{TPS}/K_{TPM} = 0.95 - 0.995$). The torque coefficients of the propeller are decreasing distinctively with the increasing of the Reynolds number ($K_{QS}/K_{QM} = 0.93 - 0.98$). The influence of the thrust loading coefficients on the propeller torque and thrust coefficients is limited in the range of $4.25 \leq C_{Th} \leq 850$.

The decrease of the propeller thrust and torque coefficients is effected by the increase of the flow velocity through the nozzle due to the higher efficiency of the nozzle at full-scale Reynolds numbers. The torque of the propeller is additionally

reduced due to the lower friction on the blades at higher Reynolds numbers. Therefore, the effect of the Reynolds number on the torque of the ducted propeller is stronger in comparison with a free running one. The tendency of a reduction of the propeller thrust at higher Reynolds numbers should also be taken into account.

The changing of the characteristic of the ducted propeller due to the Reynolds number depends on the propeller geometry (blade line, pitch and camber distribution) and the nozzle profile. The results in the Figure 20 can only demonstrate the trend and the magnitude of the Reynolds number effects for the ducted propeller DP 215-1345.

CONCLUSION

The scale effect on a ducted propeller is a complicated subject due to the interaction between the nozzle and the propeller. The numerical results confirm that CFD methods are very helpful tools for support the extrapolation of the model test results to full-scale ones.

The Reynolds number effect on the characteristic of ducted propellers can be summarised as follows:

- high reduction of the propeller torque coefficient,
- reduction of the propeller thrust coefficient,
- increase of the nozzle thrust coefficient,
- nearly unchanged total thrust coefficient.

Although the calculated results for full-scale agree with the observed tendencies in full-scale tests, more research work is needed to validate it.

ACKNOWLEDGEMENTS

The authors thank the German Ministry for Education and Research for sponsoring their research work on application of CFD methods on ducted propellers. The authors also thank Mr. Pierzynski and Mr. Lübke for their help by carrying out the numerical computations.

REFERENCES

Abdel-Maksoud, M., Menter, F. R., Wuttke, H., "Viscous Flow Simulations for Conventional and High Skew Marine Propellers", Ship Technology Research, Vol. 45, No. 2, 1998.

Abdel-Maksoud, M., "Convergence Study of Viscous Flow Computations Around a High Loaded Nozzle Propeller", Numerical Towing Tank Symposium NuTTS 2000, Tjärnö, Sweden, 2000.

Abdel-Maksoud, M., Heinke, H.-J., "Investigation of Viscous flow on modern Propulsion Systems", 95. Annual General Meeting, Schiffbautechnische Gesellschaft, Hamburg, , 2000 (in German).

Abdel-Maksoud, M., Rieck, K., Menter, F. R., "Unsteady Numerical Investigation of the Turbulent Flow Around The Container Ship Model (KCS) with and without Propeller", Gothenburg 2000, A Workshop on Numerical Ship Hydrodynamics, Gothenburg, Sweden, 2000.

Grotjans, H., Menter, F. R., "Wall Functions for General Application CFD codes", ECCOMAS 98, Fourth European Computational Fluid Dynamics Conference, Athens, 1998.

ITTC, "22nd International Towing Tank Conference", Proceedings volume II, Seoul, Korea & Shanghai, China, 1999.

Kuiper, G., "The Wageningen Propeller Series", MARIN Publication 92-001, May 1992

Menter, F. R., "Two-equation Eddy-Viscosity Turbulence Models for Engineering Applications", AIAA-Journal, Vol. 32, 1994.

Menter, F. R., Abdel-Maksoud, M., Galpin, P., "Numerical and Modelling Aspects of Flow Simulations in Rotating Machines", Proceeding of FED'98, FED SM 98-5002, ASME, , 1998.

Raw, M. J., "A Coupled Algebraic Multigrid Method for the 3D Navier-Stokes Equations in Fast Solvers for the Flow Problems", ed. W. Hackebusch, G. Wittum, Notes on Numerical Fluid Mechanics, Vol. 49, 1995.

Stierman, E.J., "Extrapolation Methods for Ships with Ducted Propeller", International Shipbuilding Progress, Vol. 31, No. 356, 1984.

Nomenclature

C_i	[ms ⁻¹]	velocity vector in the inertial system	T_N	[N]	thrust of the nozzle
C_{Th}	[-]	thrust loading coefficient	t_S	[s]	simulation time
C_{TP}	[-]	thrust loading coefficient of the propeller	T_T	[N]	total thrust
D	[m]	propeller diameter	u_T	[ms ⁻¹]	tangential velocity at the first node of the wall
L_D	[m]	diameter of calculation domain	U_i	[ms ⁻¹]	velocity vector due to the rotation of the co-ordinate system
e_{ijk}		permutation tensor	V_A	[ms ⁻¹]	inflow velocity
i		index refer to the Cartesian co-ordinate direction (i)	W_i	[ms ⁻¹]	velocity vector in the rotating system
j		index refer to the Cartesian co-ordinate direction (j)	x_i	[m]	spatial co-ordinates
k		index refer to the Cartesian co-ordinate direction (k)	y^+	[-]	dimensionless distance from the wall
K_Q	[-]	torque coefficient	λ	[-]	scale
K_{TN}	[-]	thrust coefficient of the nozzle	μ	[kqm ⁻¹ s ⁻¹]	molecular viscosity of the fluid
K_{TP}	[-]	propeller thrust coefficient	ρ	[kq m ⁻³]	density
K_{TT}	[-]	total thrust coefficient	τ_{ij}	[Nm ⁻²]	viscous stress tensor
n	[s ⁻¹]	number of revolutions	ω_i	[rads ⁻¹]	vector of system rotation
P	[Pa]	pressure	M		model
Q	[Nm]	torque of the propeller	S		full-scale
t	[s]	time			
T	[N]	thrust of the propeller			

Table 1: Influence of the applied boundary conditions on the calculated coefficients of a ducted propeller

Test case	1	2	3	4	5	Experiment
Propeller thrust coefficient K_{TP}	0.186	0.229	0.243	0.238	0.225	0.222
Torque coefficient $10K_Q$	0.363	0.387	0.372	0.365	0.381	0.373
Nozzle thrust coefficient K_{TN}	0.084	0.208	0.214	0.211	0.216	0.215
Total thrust coefficient K_{TT}	0.271	0.437	0.457	0.449	0.441	0.437
Ratio K_{TP}/K_Q	5.127	5.925	6.539	6.537	5.896	5.960
Ratio K_{TT}/K_Q	7.450	11.289	12.304	12.323	11.545	11.718
Ratio K_{TN}/K_{TP}	0.453	0.905	0.882	0.885	0.958	0.966
Thrust loading coefficient C_{Th}	621	1004	1050	1032	1012	1002
Diameter of the grid D_{calc}/D	4	9	90	90	70	-
Location of inflow plane x/D	3.5	3.5	87	87	87	-
Location of outflow plane x/D	6.5	22	130.5	130.5	130.5	-
Turbulence model	$k-\varepsilon$	$k-\varepsilon$	$k-\varepsilon$	SST	SST	-

Table 2: Data of the propeller P 1345 ($\lambda = 20$)

Type	Wageningen KA 5-75
Diameter	D [m]: 0.201
Pitch ratio	P/D [-]: 1.1867
Blade area ratio	A_E/A_O [-]: 0.750
Hub diameter ratio	d_h/D [-]: 0.1813
Number of blades	Z [-]: 5
Direction of rotation	right handed

Table 3: Data of the nozzle D 215 ($\lambda = 20$)

Type	Wageningen 19A
Nozzle length	L_D [m]: 0.10036
Diameter at propeller location	D_i [m]: 0.203
Diameter at the entrance cross-section	D_e [m]: 0.2395
Diameter at the leaving cross-section	D_a [m]: 0.2118
Radius at the entrance edge	r_e [m]: 2.8
Radius at the leaving edge	r_a [m]: 1.9
Propeller position	x_p/L_D [-]: 0.5

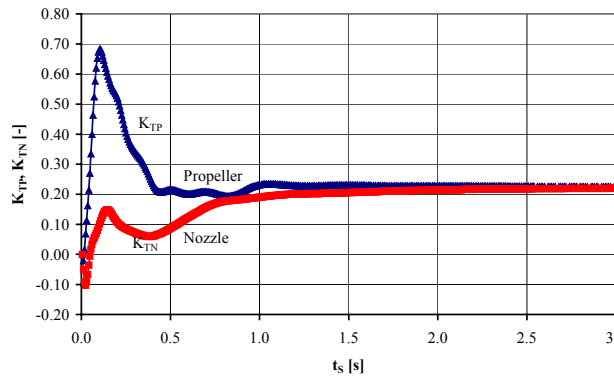


Figure 1: Variation of thrust coefficients during the simulation time t_s

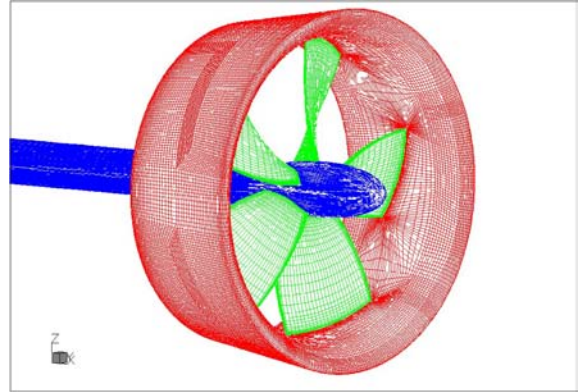


Figure 2: Numerical grid

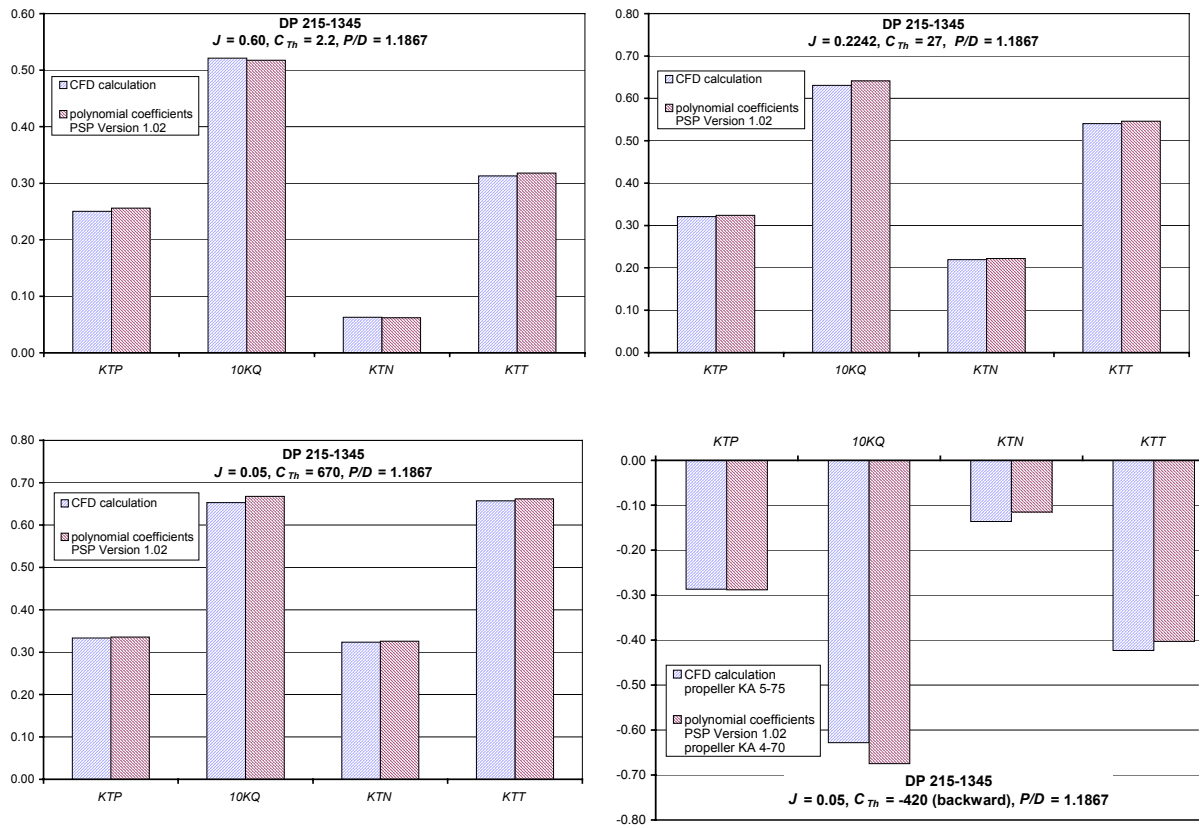


Figure 3: Comparison of the coefficients for the ducted propeller DP 215-1345 (propeller KA 5-75, nozzle Wag. 19A), numerical results and polynomial coefficients

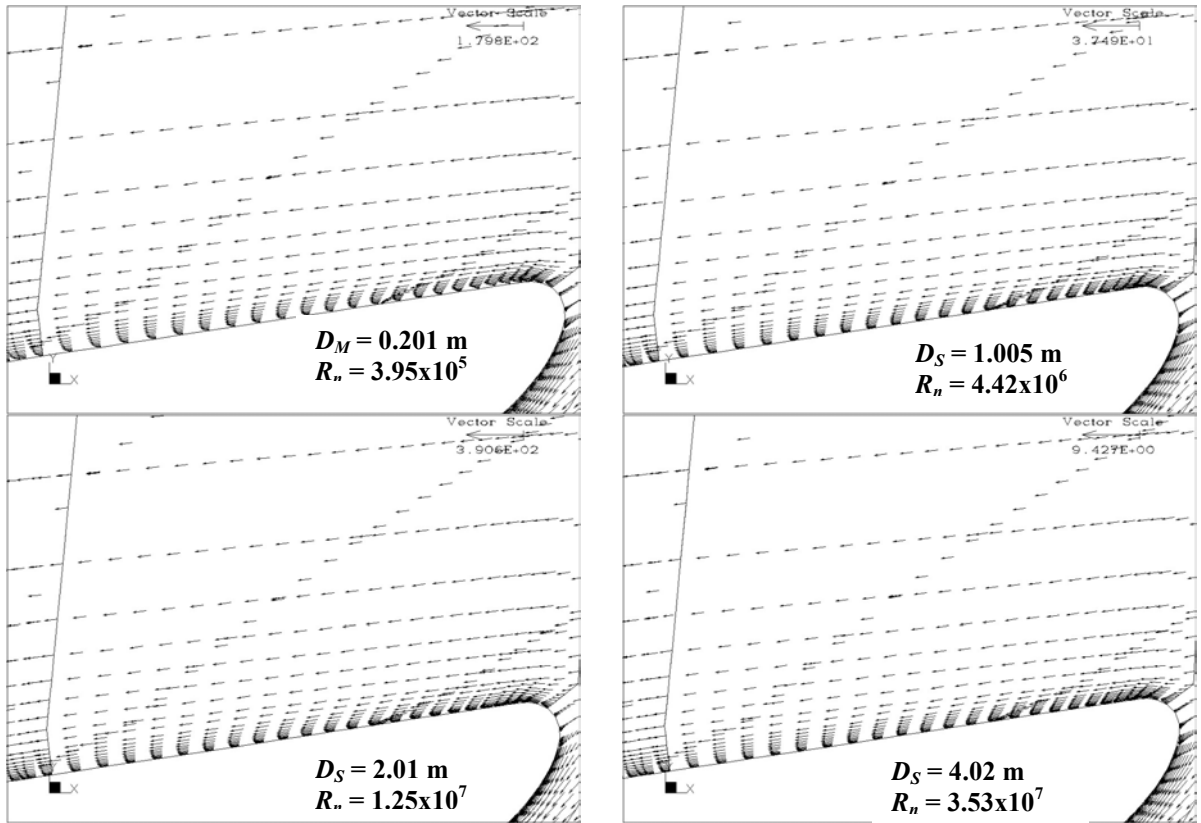


Figure 4: Velocity vectors outside the nozzle, $C_{Th} = 4.25$

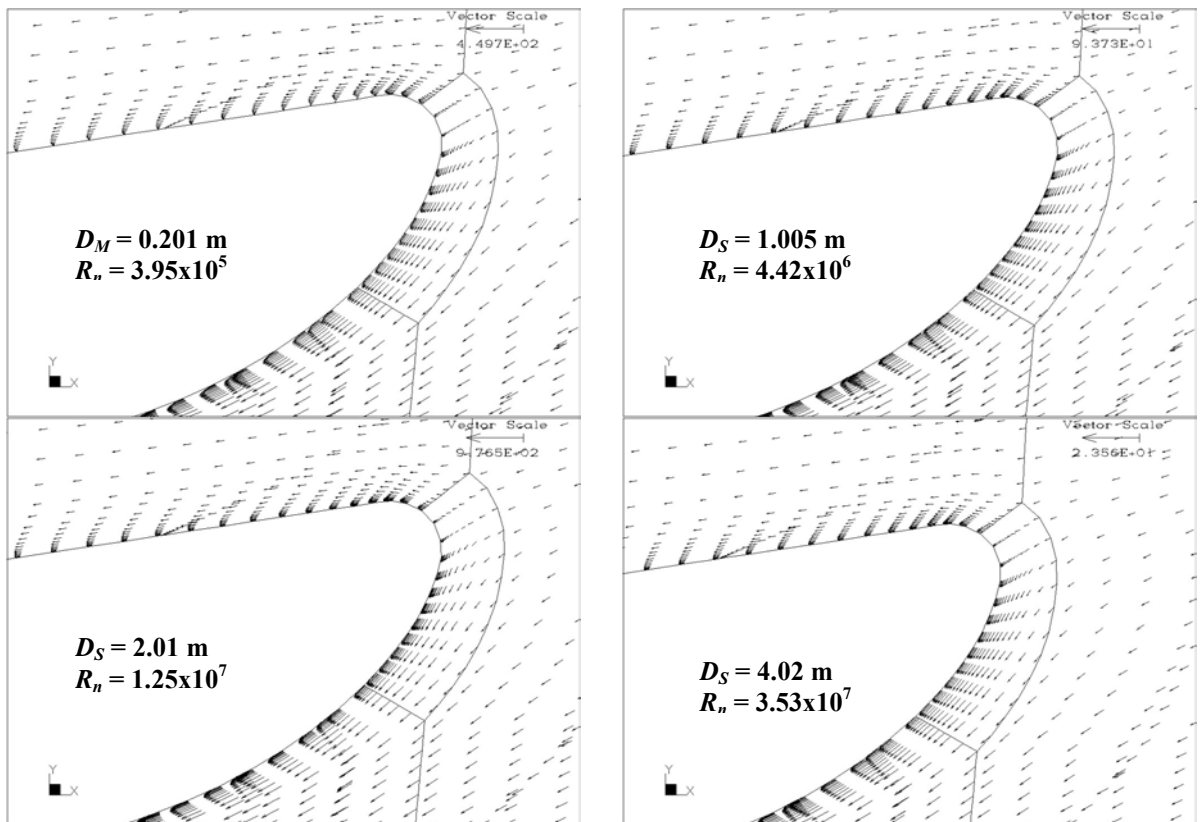


Figure 5: Velocity vectors on the nozzle leading edge, $C_{Th} = 4.25$

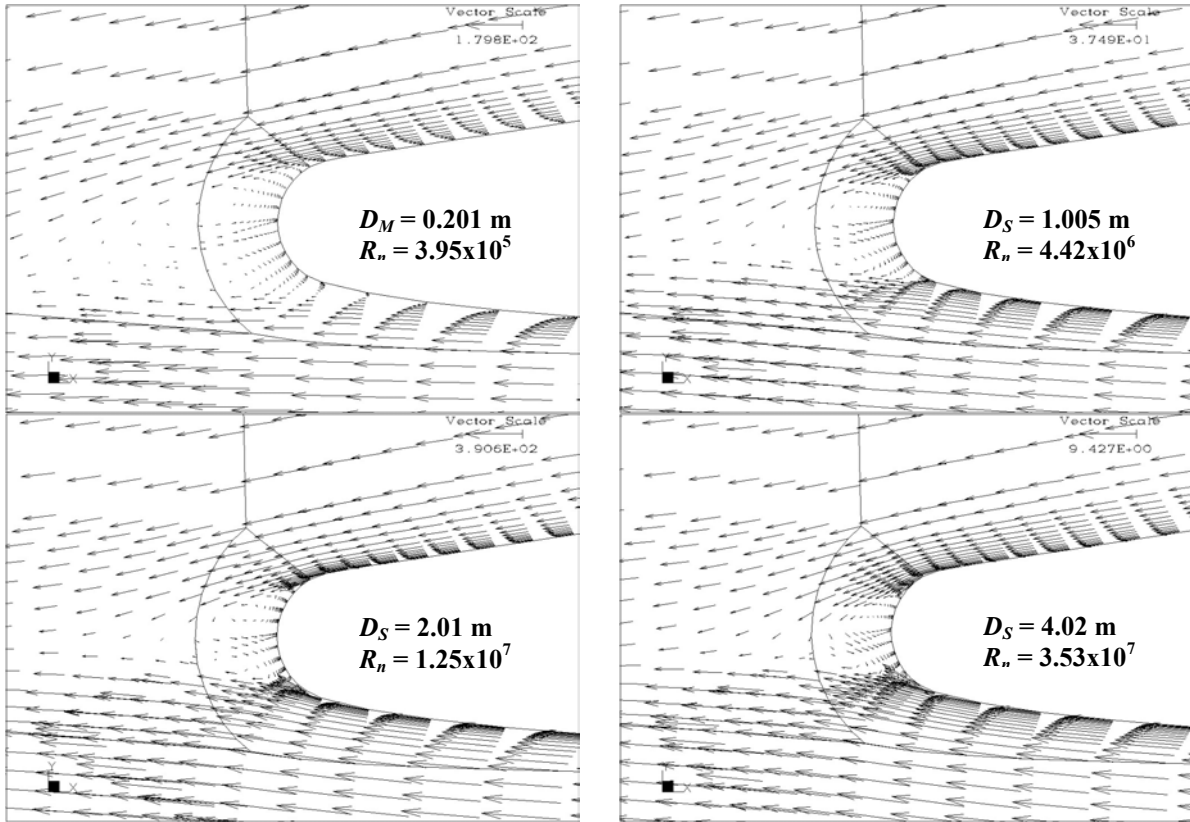


Figure 6: Velocity vectors on the nozzle trailing edge, $C_{Th} = 4.25$

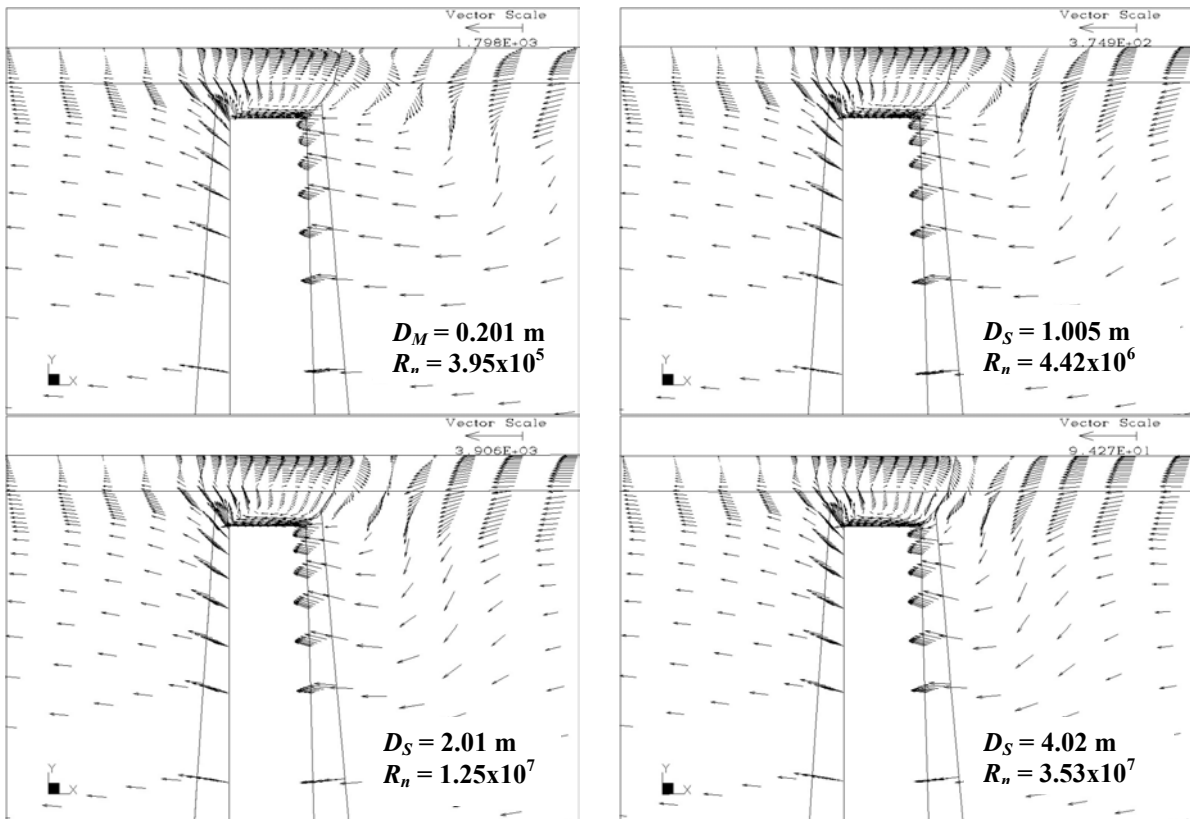


Figure 7: Velocity vectors on the propeller blade tip, $C_{Th} = 4.25$

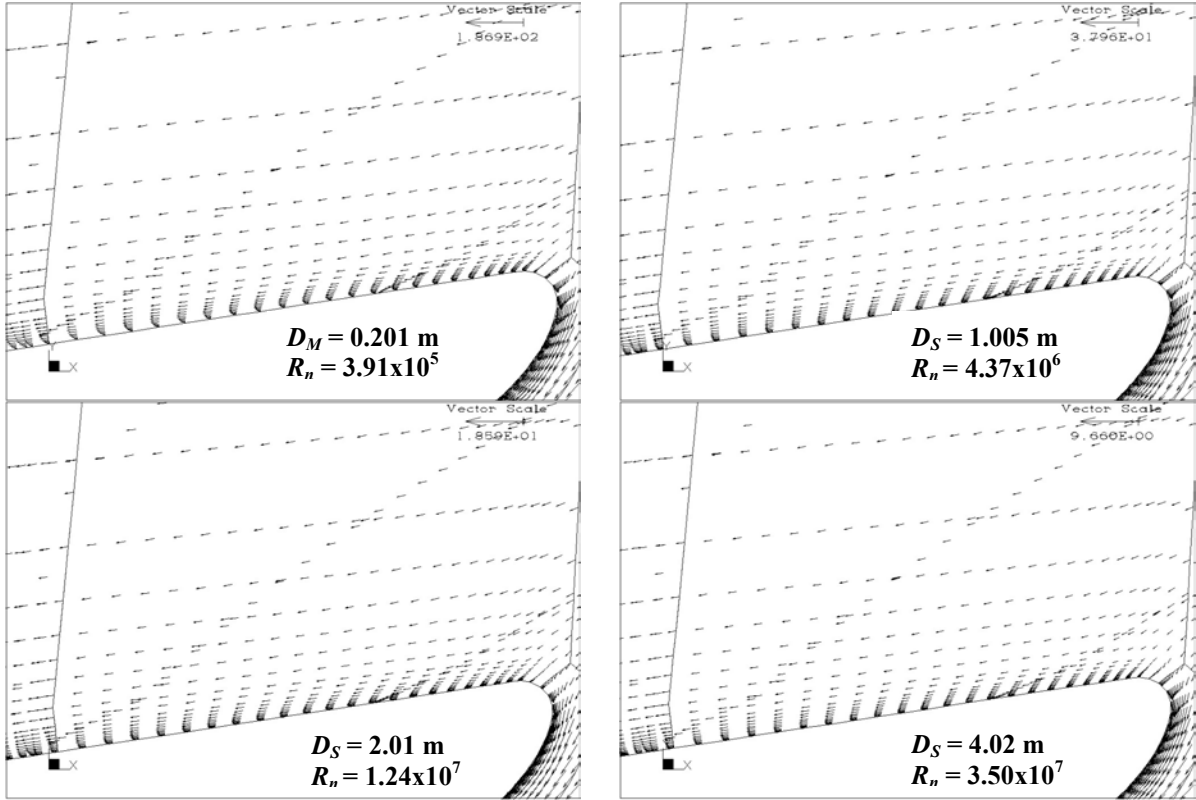


Figure 8: Velocity vectors outside the nozzle, $C_{Th} = 8.5$

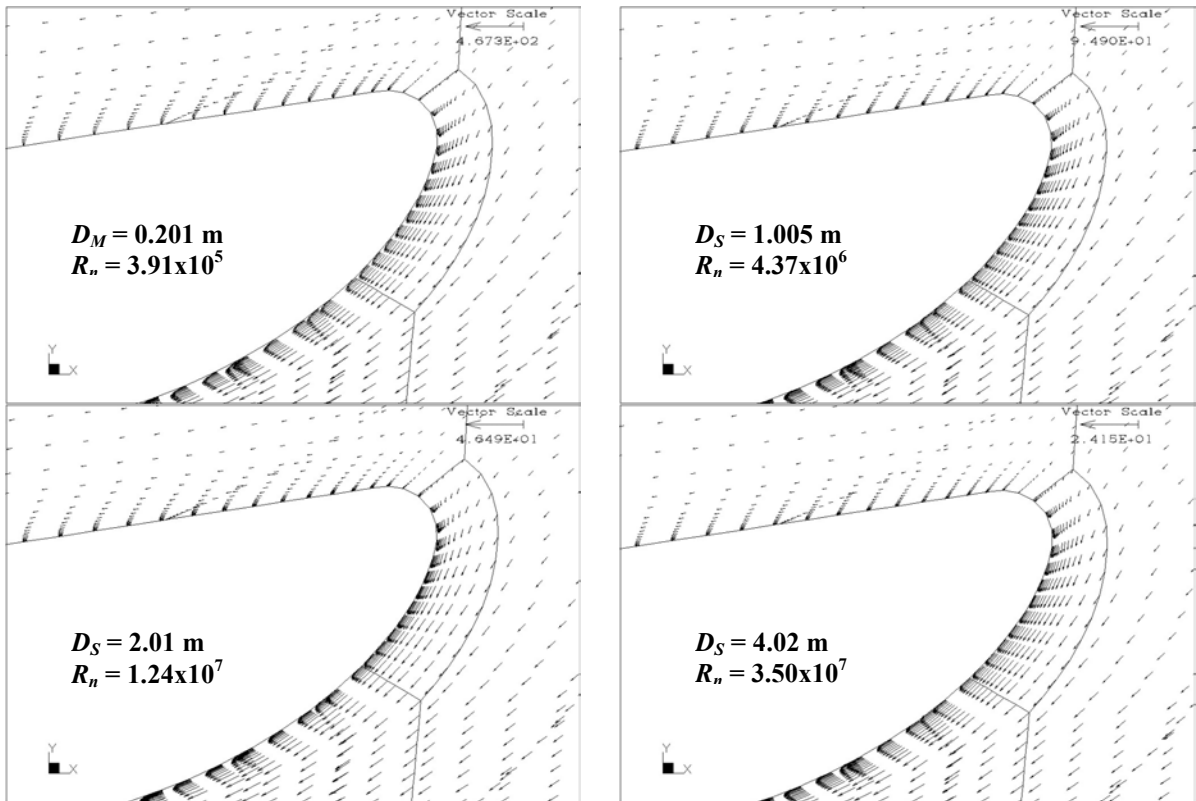


Figure 9: Velocity vectors on the nozzle leading edge, $C_{Th} = 8.5$

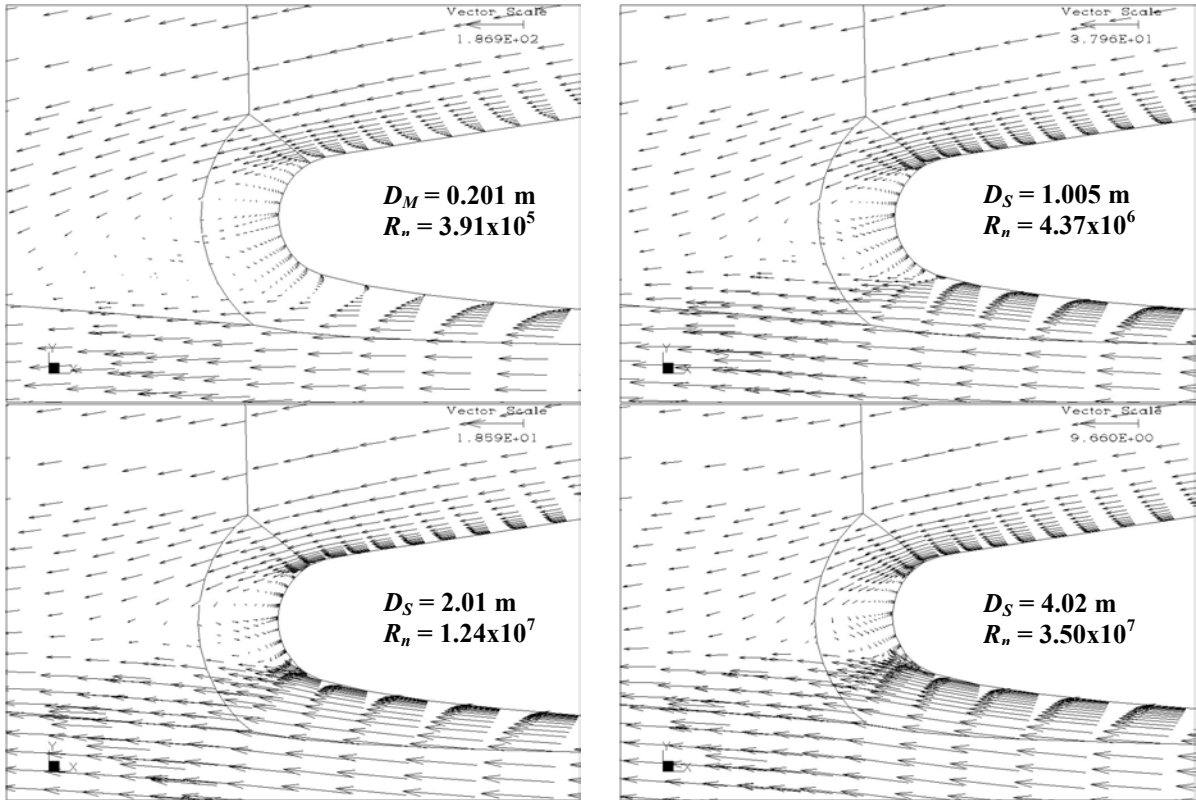


Figure 10: Velocity vectors on the nozzle trailing edge, $C_{Th} = 8.5$

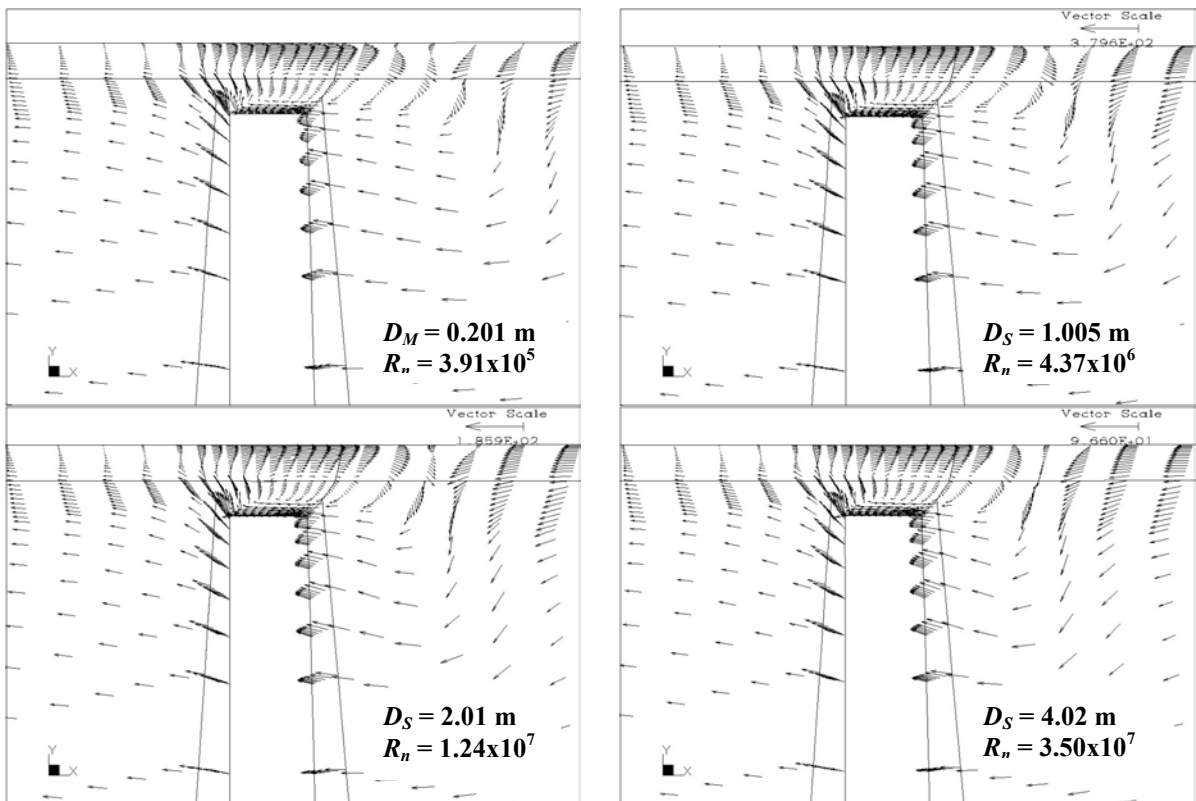


Figure 11: Velocity vectors on the propeller blade tip, $C_{Th} = 8.5$

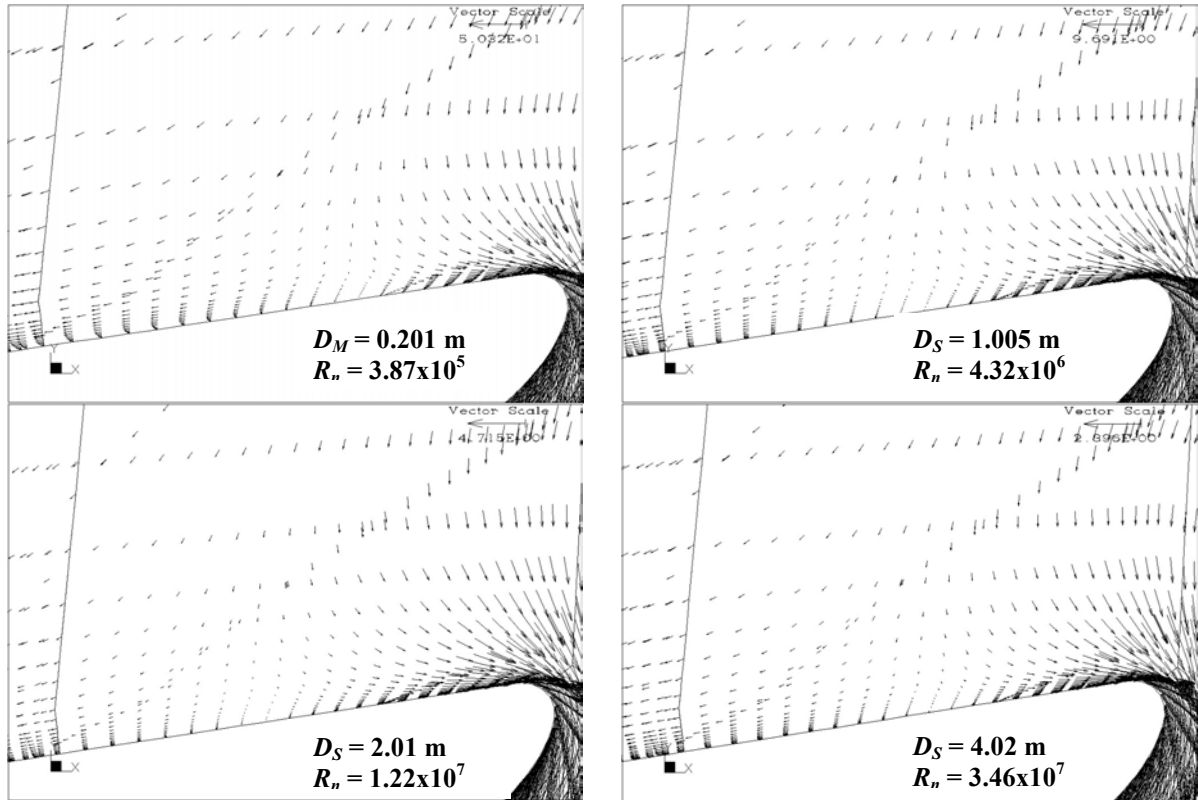


Figure 12: Velocity vectors outside the nozzle, $C_{Th} = 85$

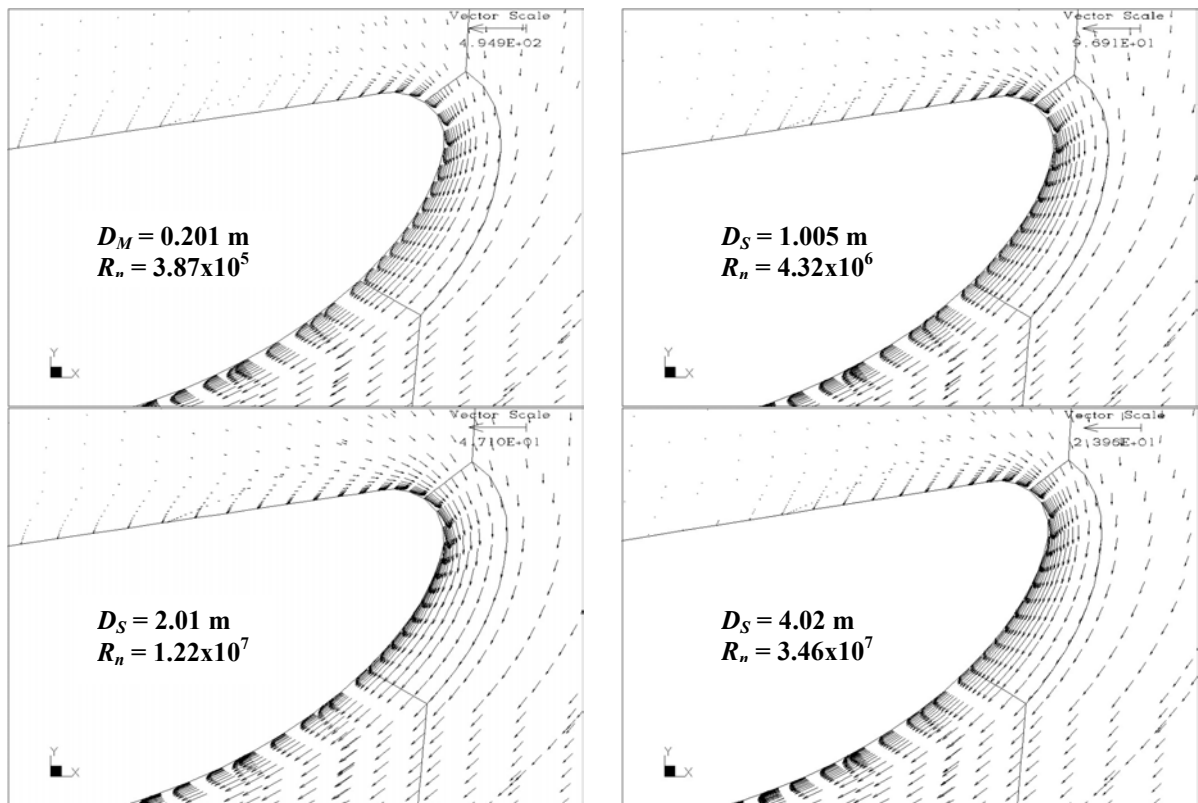


Figure 13: Velocity vectors on the nozzle leading edge, $C_{Th} = 85$

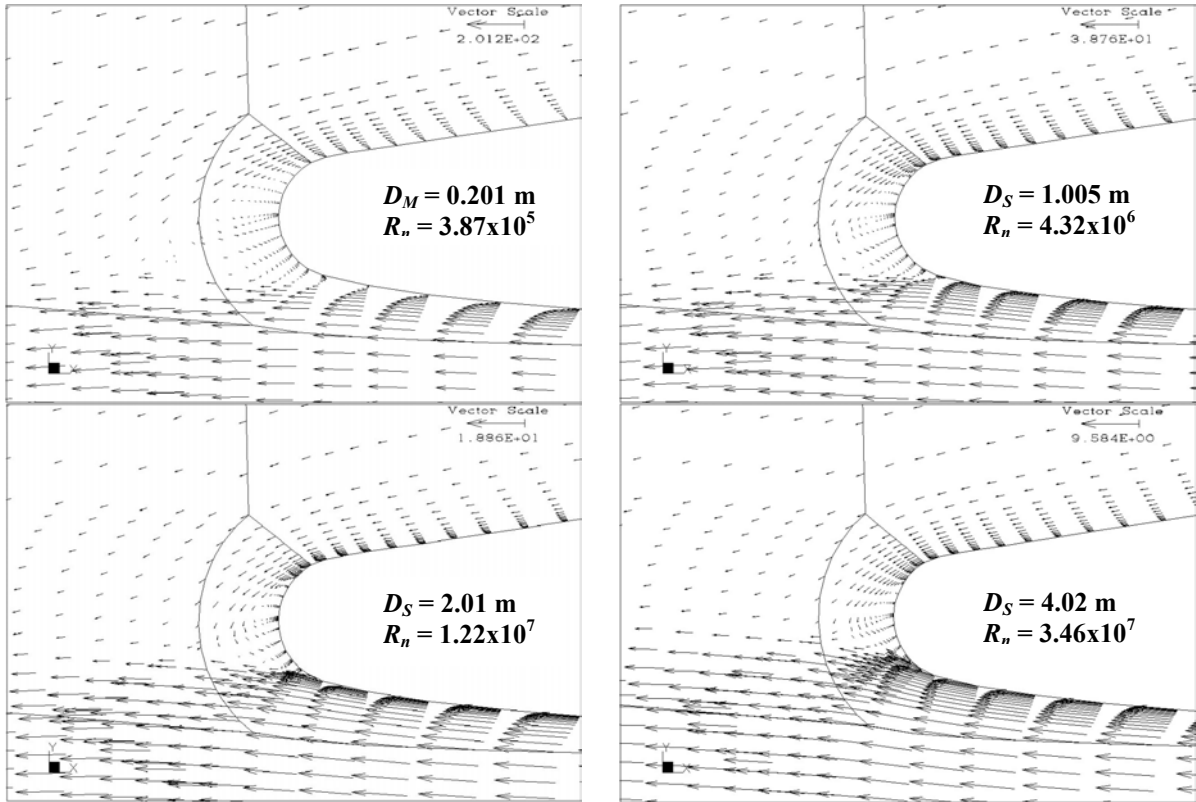


Figure 14: Velocity vectors on the nozzle trailing edge, $C_{Th} = 85$

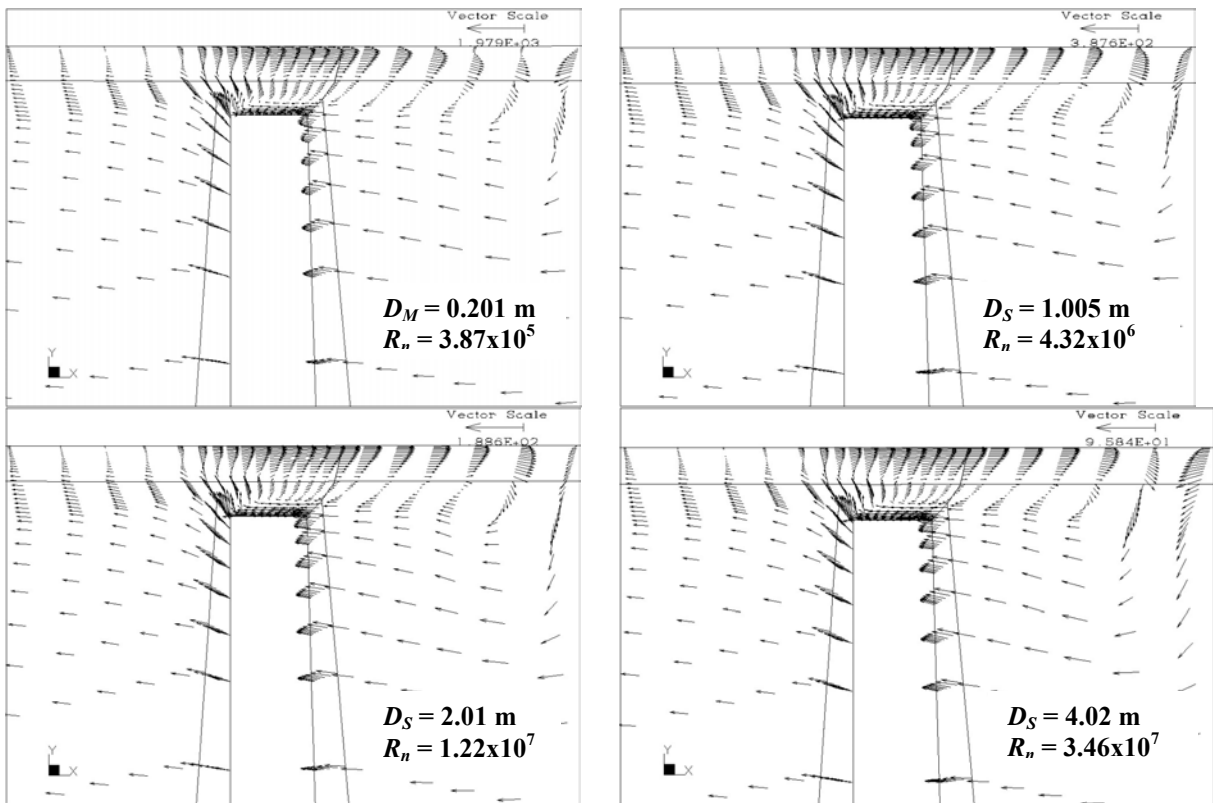


Figure 15: Velocity vectors on the propeller blade tip, $C_{Th} = 85$

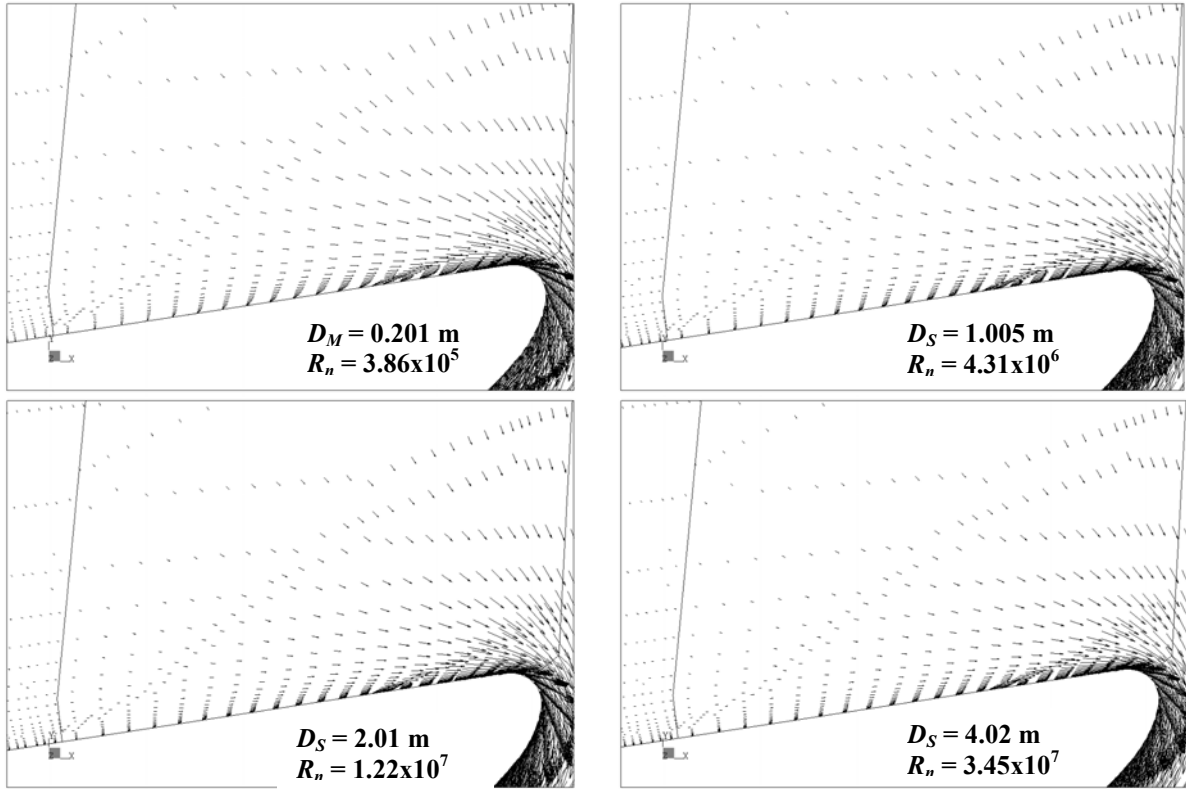


Figure 16: Velocity vectors outside the nozzle, $C_{Th} = 850$

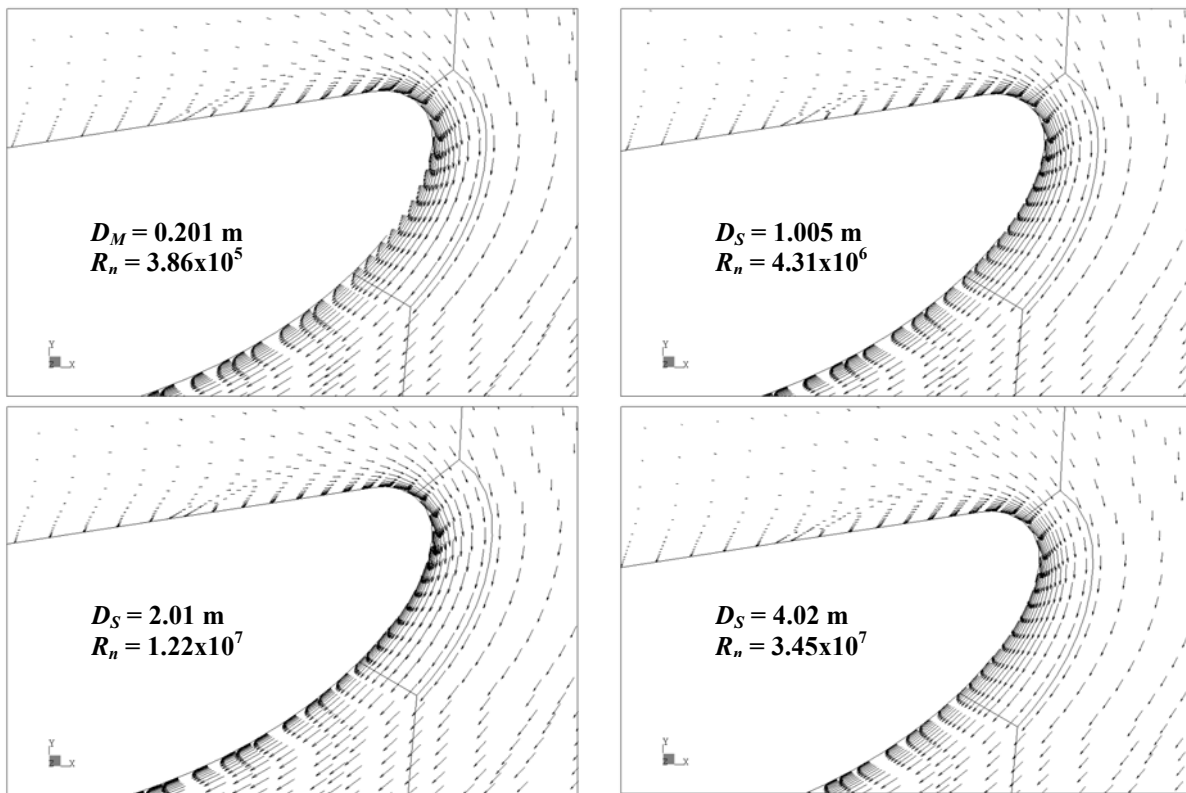


Figure 17: Velocity vectors on the nozzle leading edge, $C_{Th} = 850$

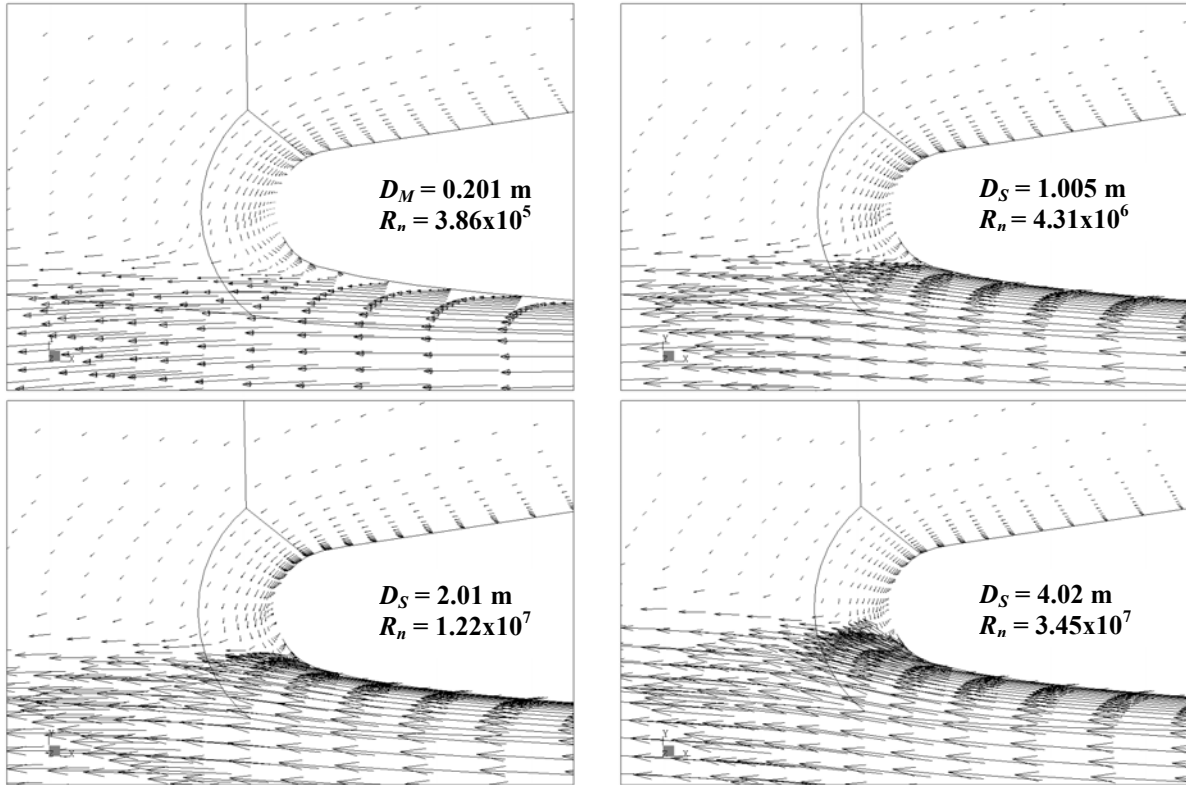


Figure 18: Velocity vectors on the nozzle trailing edge, $C_{Th} = 850$

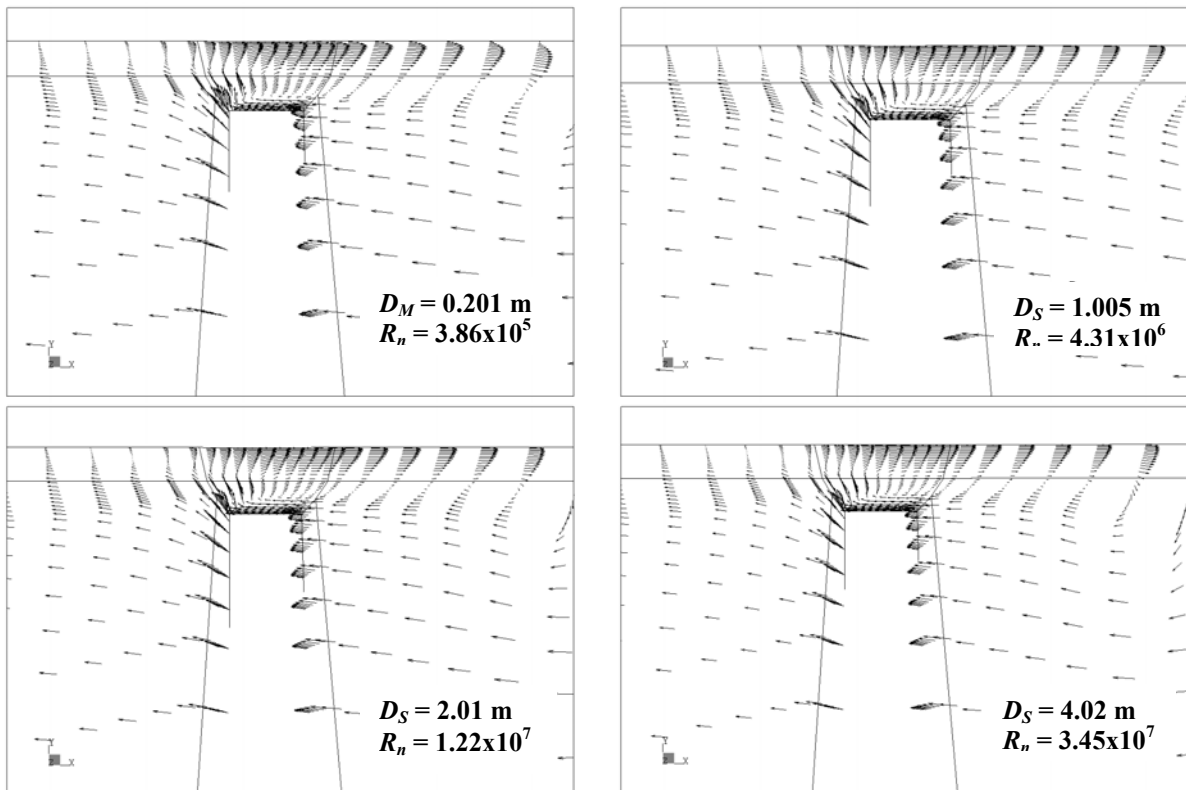


Figure 19: Velocity vectors on the propeller blade tip, $C_{Th} = 850$

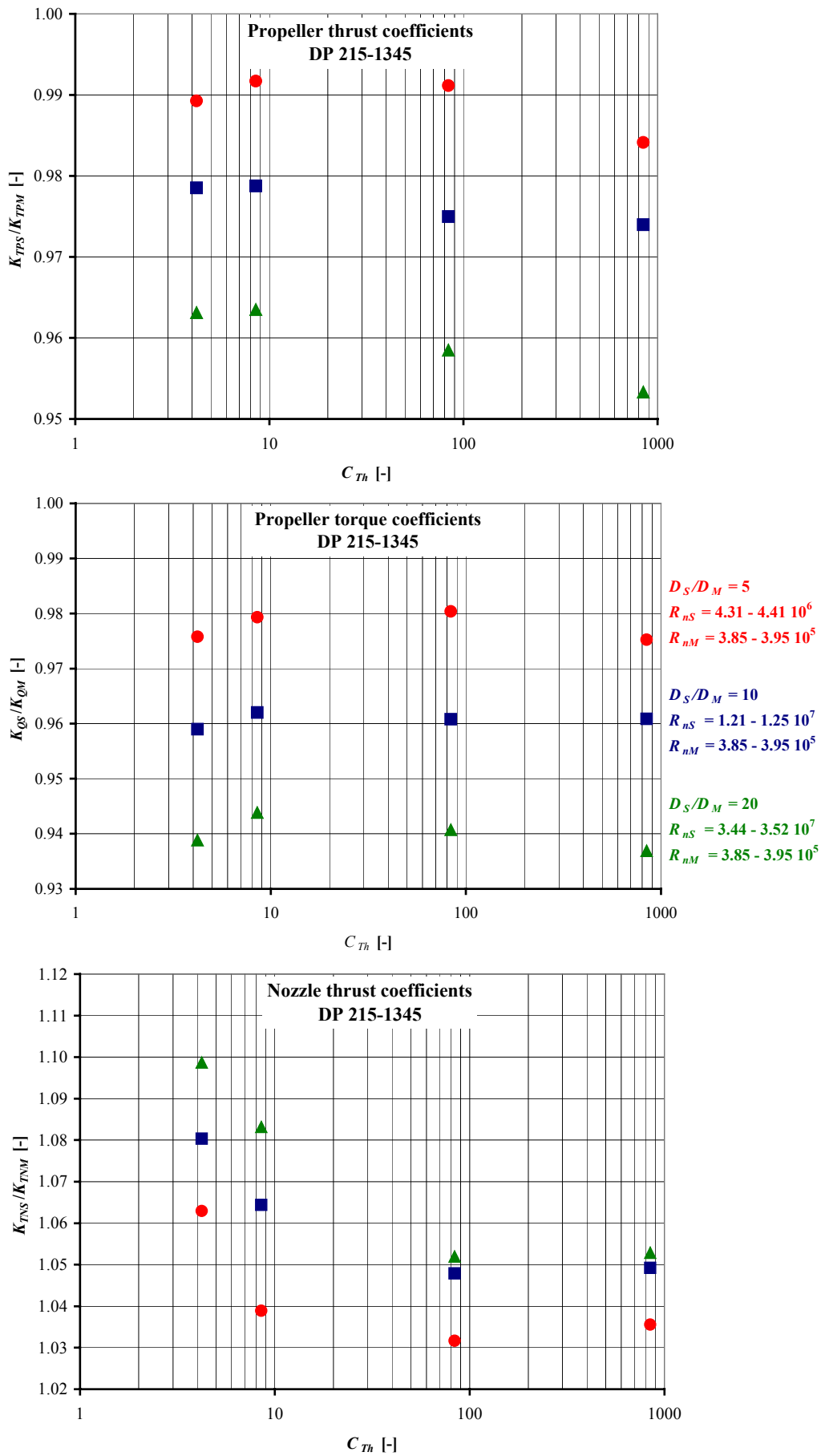


Figure 20: Influence of the Reynolds number and the thrust loading coefficient on the propeller and nozzle coefficients of the DP 215-1345 (nozzle Wag. 19A, propeller Wag. KA 5-75)